

Rotating Boson Stars and Q -Balls II: Negative Parity and Ergoregions

Burkhard Kleihaus, Jutta Kunz,
Institut für Physik, Universität Oldenburg, D-26111 Oldenburg, Germany

Meike List, Isabell Schaffer
ZARM, Universität Bremen, Am Fallturm, D-28359 Bremen, Germany

We construct axially symmetric, rotating boson stars with positive and negative parity. Their flat space limits represent spinning Q -balls. Q -balls and boson stars exist only in a limited frequency range. The coupling to gravity gives rise to a spiral-like frequency dependence of the mass and charge of boson stars. We analyze the properties of these solutions. In particular, we discuss the presence of ergoregions in boson stars, and determine their domains of existence.

PACS numbers: 04.40.-b, 11.27.+d

I. INTRODUCTION

Q -balls represent stationary localized solutions in flat space. They arise, when a complex scalar field has a suitable self-interaction [1, 2]. The global phase invariance of the scalar field theory is associated with a conserved charge Q , corresponding for instance to particle number [1].

The time-dependence of the Q -ball solutions resides in the phase of the scalar field and is associated with a frequency ω_s . Q -balls exist only in a certain frequency range, $\omega_{\min} < \omega_s < \omega_{\max}$, determined by the properties of the potential [1–5]. At a critical value of the frequency, both mass and charge of the Q -balls assume their minimal value, from where they rise monotonically towards both limiting values of the frequency. Considering the mass of the Q -balls as a function of the charge, there are thus two branches of Q -balls, merging and ending at the minimal charge and mass.

The simplest type of Q -balls is spherically symmetric. These possess finite mass and charge, but carry no angular momentum. Besides the fundamental spherically symmetric Q -balls there are also radially excited Q -balls [4]. The fundamental spherically symmetric Q -balls are stable along their lower mass branch, as long as their mass is smaller than the mass of Q free bosons [1].

Recently, the existence of rotating Q -balls was demonstrated [4, 5]. The rotation is achieved by including an additional dependence of the phase factor of the scalar field on the azimuthal angle φ , where the proportionality constant n must be integer. The resulting stationary localized Q -ball solutions then possess finite mass and finite angular momentum. Interestingly, their angular momentum J is quantized in terms of their charge Q , $J = nQ$ [4, 6]. Rotating Q -balls with $n = 1$ thus have the smallest angular momentum J for a given charge Q . The energy density and angular momentum density of rotating Q -balls possess axial symmetry. There are no (infinitesimally) slowly rotating Q -balls [4].

The field equations allow for Q -balls with positive and negative parity. The scalar field is then symmetric resp. antisymmetric w.r.t. reflections [4]. For a given charge Q one finds thus two sequences of rotating Q -balls, whose angular momentum increases with n : the positive parity sequence n^+ and the negative parity sequence n^- . While the energy density of rotating Q -balls with positive parity corresponds to a torus, the energy density of rotating Q -balls with negative parity corresponds to a double torus.

When the scalar field is coupled to gravity, boson stars arise [3, 7–9]. The presence of gravity has a crucial influence on the domain of existence of the classical solutions. Stationary spherically symmetric boson stars (0^+) also exist only in a limited frequency range, $\omega_0(\kappa) < \omega_s < \omega_{\max}$, where κ denotes the strength of the gravitational coupling. They show, however, a rather different type of frequency dependence. In particular, in the lower frequency range, the boson star solutions are not uniquely determined by the frequency. Instead a spiral-like frequency dependence of the charge and the mass is observed, where the charge and mass approach finite limiting values at the center of the spiral. Furthermore,

the charge and the mass of these boson stars tend to zero, when the maximal value of the frequency is approached [3, 7].

Rotating boson stars with positive parity have been obtained before [5, 6, 10–12]. A study of the frequency dependence of the 1^+ boson stars showed, that their frequency dependence is analogous to the one of the non-rotating 0^+ boson stars [5]. In particular, their charge and mass also exhibit a spiral structure. Like rotating Q -balls, rotating boson stars exhibit the angular momentum quantization, $J = nQ$ [6].

Here we reconsider rotating boson stars with positive parity and, for the first time, present rotating boson stars with negative parity. We construct families of boson stars of both parities numerically for constant values of the gravitational coupling strength and $n = 1$ and 2. We investigate the properties of these solutions. In particular, we analyze their frequency dependence, and we demonstrate the appearance and development of ergoregions for these families of boson star solutions [13].

In section II we recall the action, the general equations of motion and the global charges. In section III we present the stationary axially symmetric Ansatz for the metric and the scalar field, we evaluate the global charges within this Ansatz, and present the boundary conditions for the metric and scalar field function. We discuss Q -ball solutions and their properties in section IV and boson star solutions and their properties in section V. Section VI gives our conclusions.

II. ACTION, EQUATIONS AND GLOBAL CHARGES

A. Action

We consider the action of a self-interacting complex scalar field Φ coupled to Einstein gravity

$$S = \int \left[\frac{R}{16\pi G} - \frac{1}{2} g^{\mu\nu} (\Phi_{,\mu}^* \Phi_{,\nu} + \Phi_{,\nu}^* \Phi_{,\mu}) - U(|\Phi|) \right] \sqrt{-g} d^4x , \quad (1)$$

where R is the curvature scalar, G is Newton's constant, the asterisk denotes complex conjugation,

$$\Phi_{,\mu} = \frac{\partial \Phi}{\partial x^\mu} , \quad (2)$$

and U denotes the potential

$$U(|\Phi|) = \lambda |\Phi|^2 (|\Phi|^4 - a |\Phi|^2 + b) = \lambda (\phi^6 - a \phi^4 + b \phi^2) , \quad (3)$$

with $|\Phi| = \phi$. The potential is chosen such that nontopological soliton solutions [1], also referred to as Q -balls [2], exist in the absence of gravity. As seen in Fig. 1, the self-interaction of the scalar field has an attractive component, and the potential has a minimum, $U(0) = 0$, at $\Phi = 0$ and a second minimum at some finite value of $|\Phi|$. The boson mass is thus given by $m_B = \sqrt{\lambda b}$. In the numerical calculations of the solutions presented, we choose the potential parameters [4, 5]

$$\lambda = 1 , \quad a = 2 , \quad b = 1.1 . \quad (4)$$

B. Equations

Variation of the action with respect to the metric leads to the Einstein equations

$$G_{\mu\nu} = R_{\mu\nu} - \frac{1}{2} g_{\mu\nu} R = \kappa T_{\mu\nu} , \quad (5)$$

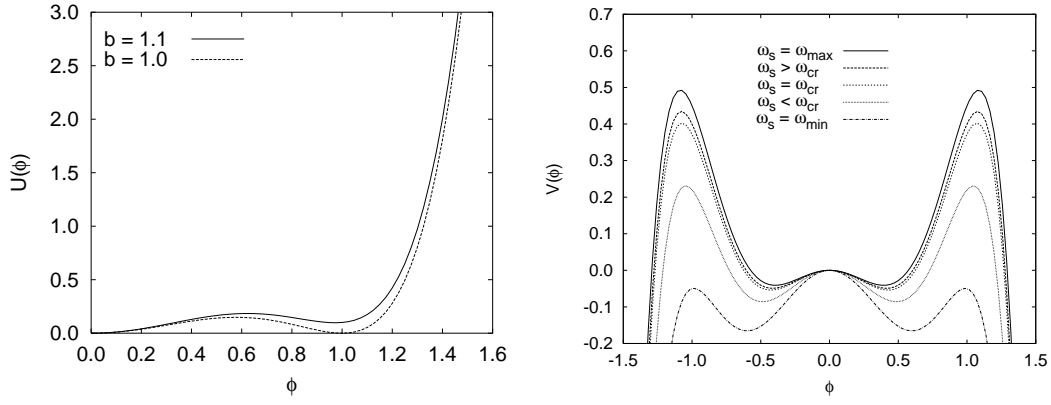


FIG. 1: Left: The potential $U(\phi)$ versus ϕ for $\lambda = 1$, $a = 2$ and $b = 1.1$ resp. $b = 1$. Right: The effective potential $V(\phi) = \frac{1}{2}\omega_s^2\phi^2 - \frac{1}{2}U(\phi)$ versus ϕ for several values of the frequency ω_s .

with $\kappa = 8\pi G$ and stress-energy tensor $T_{\mu\nu}$

$$T_{\mu\nu} = g_{\mu\nu}L_M - 2\frac{\partial L}{\partial g^{\mu\nu}} \quad (6)$$

$$= -g_{\mu\nu} \left[\frac{1}{2}g^{\alpha\beta} (\Phi_{,\alpha}^* \Phi_{,\beta} + \Phi_{,\beta}^* \Phi_{,\alpha}) + U(\phi) \right] + (\Phi_{,\mu}^* \Phi_{,\nu} + \Phi_{,\nu}^* \Phi_{,\mu}) . \quad (7)$$

Variation with respect to the scalar field leads to the matter equation,

$$\left(\square + \frac{\partial U}{\partial |\Phi|^2} \right) \Phi = 0 , \quad (8)$$

where \square represents the covariant d'Alembert operator. Equations (5) and (8) represent the general set of non-linear Einstein–Klein–Gordon equations.

C. Global Charges

The mass M and the angular momentum J of stationary asymptotically flat space-times can be obtained from their respective Komar expressions [14],

$$M = \frac{1}{4\pi G} \int_{\Sigma} R_{\mu\nu} n^{\mu} \xi^{\nu} dV , \quad (9)$$

and

$$\mathcal{J} = -\frac{1}{8\pi G} \int_{\Sigma} R_{\mu\nu} n^{\mu} \eta^{\nu} dV . \quad (10)$$

Here Σ denotes an asymptotically flat spacelike hypersurface, n^{μ} is normal to Σ with $n_{\mu}n^{\mu} = -1$, dV is the natural volume element on Σ , ξ denotes an asymptotically timelike Killing vector field and η an asymptotically spacelike Killing vector field [14]. Replacing the Ricci tensor via the Einstein equations by the stress-energy tensor yields

$$M = 2 \int_{\Sigma} \left(T_{\mu\nu} - \frac{1}{2} g_{\mu\nu} T_{\gamma}^{\gamma} \right) n^{\mu} \xi^{\nu} dV , \quad (11)$$

and

$$\mathcal{J} = - \int_{\Sigma} \left(T_{\mu\nu} - \frac{1}{2} g_{\mu\nu} T_{\gamma}^{\gamma} \right) n^{\mu} \eta^{\nu} dV . \quad (12)$$

A conserved charge Q is associated with the complex scalar field Φ , since the Lagrange density is invariant under the global phase transformation

$$\Phi \rightarrow \Phi e^{i\alpha} , \quad (13)$$

leading to the conserved current

$$j^\mu = -i(\Phi^* \partial^\mu \Phi - \Phi \partial^\mu \Phi^*) , \quad j^\mu_{;\mu} = 0 . \quad (14)$$

III. ANSATZ AND BOUNDARY CONDITIONS

A. Ansatz

To obtain stationary axially symmetric solutions, we impose on the space-time the presence of two commuting Killing vector fields, ξ and η , where

$$\xi = \partial_t , \quad \eta = \partial_\varphi \quad (15)$$

in a system of adapted coordinates $\{t, r, \theta, \varphi\}$. In these coordinates the metric is independent of t and φ , and can be expressed in isotropic coordinates in the Lewis–Papapetrou form [15]

$$ds^2 = -f dt^2 + \frac{l}{f} \left[h (dr^2 + r^2 d\theta^2) + r^2 \sin^2 \theta \left(d\varphi - \frac{\omega}{r} dt \right)^2 \right] . \quad (16)$$

The four metric functions f, l, h and ω are functions of the variables r and θ only.

The symmetry axis of the spacetime, where $\eta = 0$, corresponds to the z -axis. The elementary flatness condition [16]

$$\frac{X_{;\mu} X^{;\mu}}{4X} = 1 , \quad X = \eta^\mu \eta_\mu \quad (17)$$

then imposes on the symmetry axis the condition [17]

$$h|_{\theta=0} = h|_{\theta=\pi} = 1 . \quad (18)$$

For the scalar field Φ we adopt the stationary Ansatz [6]

$$\Phi(t, r, \theta, \varphi) = \phi(r, \theta) e^{i\omega_s t + i n \varphi} , \quad (19)$$

where $\phi(r, \theta)$ is a real function, and ω_s and n are real constants. Single-valuedness of the scalar field requires

$$\Phi(\varphi) = \Phi(2\pi + \varphi) , \quad (20)$$

thus the constant n must be an integer, i.e., $n = 0, \pm 1, \pm 2, \dots$. We refer to n as the rotational quantum number. When $n \neq 0$, the phase factor $\exp(in\varphi)$ prevents spherical symmetry of the scalar field Φ .

Solutions with positive and negative parity satisfy, respectively,

$$\phi(r, \pi - \theta) = \phi(r, \theta) \quad (21)$$

$$\phi(r, \pi - \theta) = -\phi(r, \theta) , \quad (22)$$

To construct stationary axially symmetric boson star solutions a system of five coupled partial differential equations needs to be solved. In contrast, for Q -balls the metric is the Minkowski metric, i.e., $f = l = h = 1, \omega = 0$. Here, at least in principle, only a single partial differential equation for the scalar field function needs to be solved.

B. Mass, angular momentum and charge

The mass M and the angular momentum J can be read off the asymptotic expansion of the metric functions f and ω , respectively, [15]

$$f = 1 - \frac{2MG}{r} + O\left(\frac{1}{r^2}\right), \quad \omega = \frac{2JG}{r^2} + O\left(\frac{1}{r^3}\right), \quad (23)$$

i.e.,

$$M = \frac{1}{2G} \lim_{r \rightarrow \infty} r^2 \partial_r f, \quad J = \frac{1}{2G} \lim_{r \rightarrow \infty} r^2 \omega. \quad (24)$$

This is seen by considering the Komar expressions Eqs. (9) and (10), with unit vector $n^\mu = (1, 0, 0, \omega/r)/\sqrt{f}$, and volume element $dV = 1/\sqrt{f}|g|^{1/2} dr d\theta d\varphi$, leading to [18]

$$\begin{aligned} M &= -\frac{1}{8\pi G} \int_{\Sigma} R_t^t \sqrt{-g} dr d\theta d\varphi \\ &= \lim_{r \rightarrow \infty} \frac{2\pi}{8\pi G} \int_0^\pi \left[\frac{\sqrt{l}}{f} r^2 \sin \theta \left(\frac{\partial f}{\partial r} - \frac{l}{f} \sin^2 \theta \omega \left(\frac{\partial \omega}{\partial r} - \frac{\omega}{r} \right) \right) \right] \Big|_r d\theta, \end{aligned} \quad (25)$$

and similarly

$$J = \lim_{r \rightarrow \infty} \frac{2\pi}{16\pi G} \int_0^\pi \left[\frac{l^{3/2}}{f^2} r^2 \sin^3 \theta \left(\omega - r \frac{\partial \omega}{\partial r} \right) \right] \Big|_r d\theta. \quad (26)$$

Insertion of the asymptotic expansions of the metric functions then yields expressions (24).

Alternatively, the mass M and the angular momentum J can be obtained by direct integration of the expressions (11) and (12), where

$$\begin{aligned} M &= \int_{\Sigma} (2T_\mu^\nu - \delta_\mu^\nu T_\gamma^\gamma) n_\nu \xi^\mu dV, \\ &= \int (2T_t^t - T_\mu^\mu) |g|^{1/2} dr d\theta d\varphi, \end{aligned} \quad (27)$$

corresponds to the Tolman mass, and

$$J = - \int T_\varphi^t |g|^{1/2} dr d\theta d\varphi. \quad (28)$$

The conserved scalar charge Q is obtained from the time-component of the current,

$$\begin{aligned} Q &= - \int j^t |g|^{1/2} dr d\theta d\varphi \\ &= 4\pi\omega_s \int_0^\infty \int_0^\pi |g|^{1/2} \frac{1}{f} \left(1 + \frac{n}{\omega_s} \frac{\omega}{r} \right) \phi^2 dr d\theta. \end{aligned} \quad (29)$$

From Eq. (28) for the angular momentum J and Eq. (29) for the scalar charge Q , one obtains the important quantization relation for the angular momentum,

$$J = nQ, \quad (30)$$

first derived by Schunck and Mielke [6], by taking into account that $T_\varphi^t = nj^t$, since $\partial_\varphi \Phi = in\Phi$. Thus a boson star with $n = 0$ carries no angular momentum, $J = 0$.

C. Boundary conditions

The choice of appropriate boundary conditions must guarantee that the boson star solutions are globally regular and asymptotically flat, and that they possess finite energy and finite energy density.

For rotating axially symmetric boson stars appropriate boundary conditions must be specified for the metric functions $f(r, \theta)$, $l(r, \theta)$, $h(r, \theta)$ and $\omega(r, \theta)$, and the scalar field function $\phi(r, \theta)$ at infinity, at the origin, on the positive z -axis ($\theta = 0$), and, exploiting the reflection properties w.r.t. $\theta \rightarrow \pi - \theta$, in the xy -plane ($\theta = \pi/2$).

For $r \rightarrow \infty$ the metric approaches the Minkowski metric $\eta_{\alpha\beta}$ and the scalar field assumes its vacuum value $\Phi = 0$. Accordingly, we impose at infinity the boundary conditions

$$f|_{r \rightarrow \infty} = 1, \quad l|_{r \rightarrow \infty} = 1, \quad h|_{r \rightarrow \infty} = 1, \quad \omega|_{r \rightarrow \infty} = 0, \quad \phi|_{r \rightarrow \infty} = 0. \quad (31)$$

At the origin we require

$$\partial_r f|_{r=0} = 0, \quad \partial_r l|_{r=0} = 0, \quad h|_{r=0} = 1, \quad \omega|_{r=0} = 0, \quad \phi|_{r=0} = 0. \quad (32)$$

Note, that for spherically symmetric boson stars the scalar field has a finite value ϕ_0 at the origin, though.

For $\theta = 0$ and $\theta = \pi/2$, respectively, we require the boundary conditions

$$\partial_\theta f|_{\theta=0} = 0, \quad \partial_\theta l|_{\theta=0} = 0, \quad h|_{\theta=0} = 1, \quad \partial_\theta \omega|_{\theta=0} = 0, \quad \phi|_{\theta=0} = 0, \quad (33)$$

and

$$\partial_\theta f|_{\theta=\pi/2} = 0, \quad \partial_\theta l|_{\theta=\pi/2} = 0, \quad \partial_\theta h|_{\theta=\pi/2} = 0, \quad \partial_\theta \omega|_{\theta=\pi/2} = 0, \quad \partial_\theta \phi|_{\theta=\pi/2} = 0, \quad (34)$$

for even parity solutions, while for odd parity solutions $\phi|_{\theta=\pi/2} = 0$.

In non-rotating solutions, the metric function ω is identically zero. In spherically symmetric solutions the functions depend on the radial coordinate only, with metric function $h = 1$. For the flat space solutions the metric corresponds to the Minkowski metric everywhere.

D. Numerical method

Rotating solutions are obtained when $n \neq 0$. The resulting set of coupled non-linear partial differential equations is solved numerically [19] subject to the above boundary conditions, Eqs. (31)-(34). Because of the power law fall-off of the metric functions, we compactify space by introducing the compactified radial coordinate

$$\bar{r} = \frac{r}{1+r}. \quad (35)$$

The numerical calculations are based on the Newton-Raphson method. The equations are discretized on a non-equidistant grid in \bar{r} and θ . Typical grids used have sizes 90×70 , covering the integration region $0 \leq \bar{r} \leq 1$ and $0 \leq \theta \leq \pi/2$.

IV. Q-BALLS

A. Spherically symmetric Q-balls

We first briefly review the main features of spherically symmetric Q -balls (see e.g. [1, 2, 4], or [3] for a review). The equation of motion for spherically symmetric Q -balls is given by

$$0 = \phi'' + \frac{2}{r} \phi' - \frac{1}{2} \frac{dU(\phi)}{d\phi} + \omega_s^2 \phi. \quad (36)$$

It may be interpreted to effectively describe a particle moving with friction in the effective potential

$$V(\phi) = \frac{1}{2} \omega_s^2 \phi^2 - \frac{1}{2} U(\phi), \quad (37)$$

exhibited in Fig. 1.

Q -balls exist in the frequency range

$$\omega_{\min}^2 < \omega_s^2 < \omega_{\max}^2, \quad (38)$$

where the maximal frequency ω_{\max} and the minimal frequency ω_{\min} are determined by the properties of the potential U [4],

$$\omega_s^2 < \omega_{\max}^2 \equiv \frac{1}{2}U''(0) = \lambda b, \quad (39)$$

$$\omega_s^2 > \omega_{\min}^2 \equiv \min_{\phi} [U(\phi)/\phi^2] = \lambda \left(b - \frac{a^2}{4} \right). \quad (40)$$

The mass M of the Q -balls can be obtained from

$$M = 4\pi \int_0^\infty [\omega_s^2 \phi^2 + \phi'^2 + U(\phi)] r^2 dr, \quad (41)$$

where the prime denotes differentiation with respect to r , and and their charge Q from

$$Q(\omega_s) = 8\pi \omega_s \int_0^\infty \phi^2 r^2 dr. \quad (42)$$

Fixing the value of ω_s in the allowed range, one then obtains a sequence of Q -ball solutions, consisting of the fundamental Q -ball and its radial excitations [4]. The boson function ϕ of the fundamental Q -ball has no nodes, while it has k nodes for the k -th radial excitation.

We exhibit the fundamental Q -ball solution ($k = 0$) and the first radial excitation ($k = 1$) in Fig. 2. Here the charge Q is shown versus the frequency ω_s . As seen in the figure, at a critical value ω_{cr} , which depends on k , the charge assumes its respective minimal value Q_{cr} . Thus two branches of solutions exist for each k , the lower branch $\omega_s < \omega_{\text{cr}}$ and the upper branch $\omega_s > \omega_{\text{cr}}$, which merge and end at ω_{cr} . When $\omega_s \rightarrow \omega_{\min}$ as well as when $\omega_s \rightarrow \omega_{\max}$ the charge diverges [1].

In Fig. 2 also the mass M of these two sets of solutions is shown, but it is now exhibited versus the charge Q . The lower mass branches correspond to the lower values of the frequency, $\omega_s < \omega_{\text{cr}}$, while the upper mass branches correspond to higher values of the frequency, $\omega_s > \omega_{\text{cr}}$. As long as the mass is smaller than the mass of Q free bosons, $M < m_B Q$, the fundamental Q -ball solutions are stable, both classically and quantum mechanically [1]. Classically the solutions remain stable all along the lower branch. The classical stability changes only at the critical point, Q_{cr} , where the solutions acquire an unstable mode [1]. In contrast, from a quantum perspective the stability changes when the lower mass branch intersects the line corresponding to the mass of Q free bosons. On the unstable upper branch the mass approaches the mass $M = m_B Q$ of Q free bosons from above, as $\omega_s \rightarrow \omega_{\max}$ [1].

We remark, that also angularly excited non-rotating Q -balls have been obtained recently [20]. These new solutions are axially symmetric, and their angular dependence is given by spherical harmonics. They have higher energy and charge than the spherically symmetric Q -balls, but lower energy and charge than the rotating Q -balls. In addition, interacting Q -balls have been studied [20].

B. Rotating Q -balls

The existence of rotating Q -balls was shown by Volkov and Wöhnert [4]. Based on the Ansatz (19) for the scalar field Φ [6], rotating Q -balls are solutions of the field equation

$$\left(\frac{\partial^2}{\partial r^2} + \frac{2}{r} \frac{\partial}{\partial r} + \frac{1}{r^2} \frac{\partial^2}{\partial \theta^2} + \frac{\cos \theta}{r^2 \sin \theta} \frac{\partial}{\partial \theta} - \frac{n^2}{r^2 \sin^2 \theta} + \omega_s^2 \right) \phi = \frac{1}{2} \frac{dU(\phi)}{d\phi}, \quad (43)$$

with mass [4]

$$M = 2\pi \int_0^\infty \int_0^\pi \left(\omega_s^2 \phi^2 + (\partial_r \phi)^2 + \frac{1}{r^2} (\partial_\theta \phi)^2 + \frac{n^2 \phi^2}{r^2 \sin^2 \theta} + U(\phi) \right) r^2 dr \sin \theta d\theta, \quad (44)$$

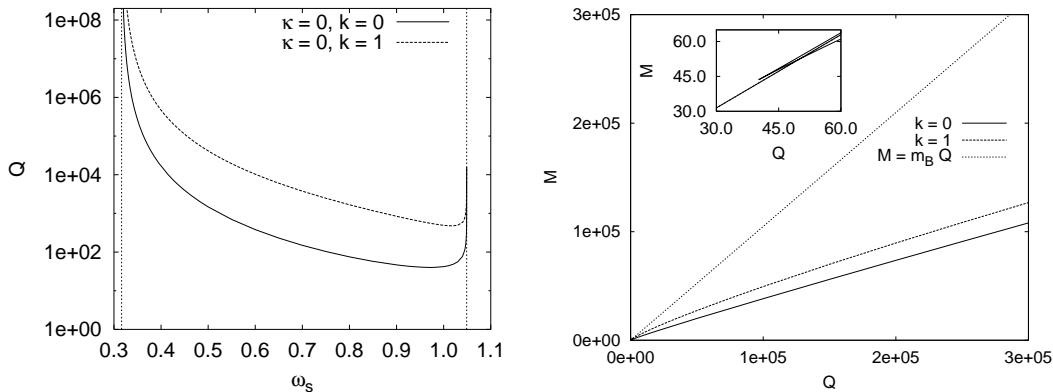


FIG. 2: Left: The charge Q versus the frequency ω_s for spherically symmetric fundamental Q -balls ($k = 0$) and their first radial excitations ($k = 1$). Also shown are the limiting values of the frequency, ω_{\min} and ω_{\max} . Right: The mass M versus the charge Q for spherically symmetric fundamental Q -balls ($k = 0$) and their first radial excitations ($k = 1$). Also shown is the mass for Q free bosons, $M = m_B Q$. The mass on the upper branches is very close this mass. The $k = 0$ branches close to the critical charge Q_{cr} are seen in the inset.

and charge

$$Q = 4\pi\omega_s \int_0^\infty \int_0^\pi \phi^2 r^2 dr \sin\theta d\theta . \quad (45)$$

Their angular momentum satisfies the quantization relation $J = nQ$.

In their pioneering study [4] Volkov and Wöhnert showed, that for a given value of n there are two types of solutions, positive parity Q -balls n^+ and negative parity Q -balls n^- . In the following we restrict our considerations to fundamental rotating Q -balls.

1. Positive parity Q -balls

We first recall the properties of rotating Q -balls with positive parity and, at the same time, extend the previous studies [4, 5] to higher rotational quantum number n . In Fig. 3 we illustrate the scalar field ϕ and the energy density T_{tt} of rotating Q -balls with charge $Q = 410$, $n^P = 1^+, 2^+$ and 3^+ . For rotating Q -balls the scalar field ϕ vanishes on the z -axis. The energy density T_{tt} of even parity rotating Q -balls typically exhibits a torus-like structure. This torus-like shape becomes apparent by considering surfaces of constant energy density of e.g. half the respective maximal value of the energy density. As seen in the figure, the maximum of the energy density increases and shifts towards larger values of the coordinate $\rho = r \sin\theta$, when n and thus the angular momentum increases. In terms of the energy density tori this manifests as an increase of their radii in the equatorial plane with increasing n . (Note, that in [5] a weighted energy density was shown.)

We next address the frequency dependence for these rotating Q -ball solutions with positive parity. In Fig. 4 we exhibit the charge Q versus the frequency ω_s for Q -balls with $n = 0 - 3$. We observe the same upper limiting value ω_{\max} , Eq. (39), for the frequency ω_s , as for non-rotating Q -balls, ensuring asymptotically an exponential fall-off of the scalar field ϕ . For a given frequency ω_s the charge of a Q -ball increases with n . We thus conclude, that the frequency of rotating Q -balls is limited by the minimal frequency ω_{\min} , Eq. (40), as well, independent of n .

The mass of these rotating Q -balls with positive parity shows the same critical behaviour and thus cusp structure as the mass of the non-rotating Q -balls. This is also illustrated in Fig. 4. Thus we conclude, that these rotating solutions are classically stable along their lower mass branches. Overall we note, that the sets of rotating Q -balls with positive parity exhibit the same general pattern as the sets of non-rotating Q -balls.

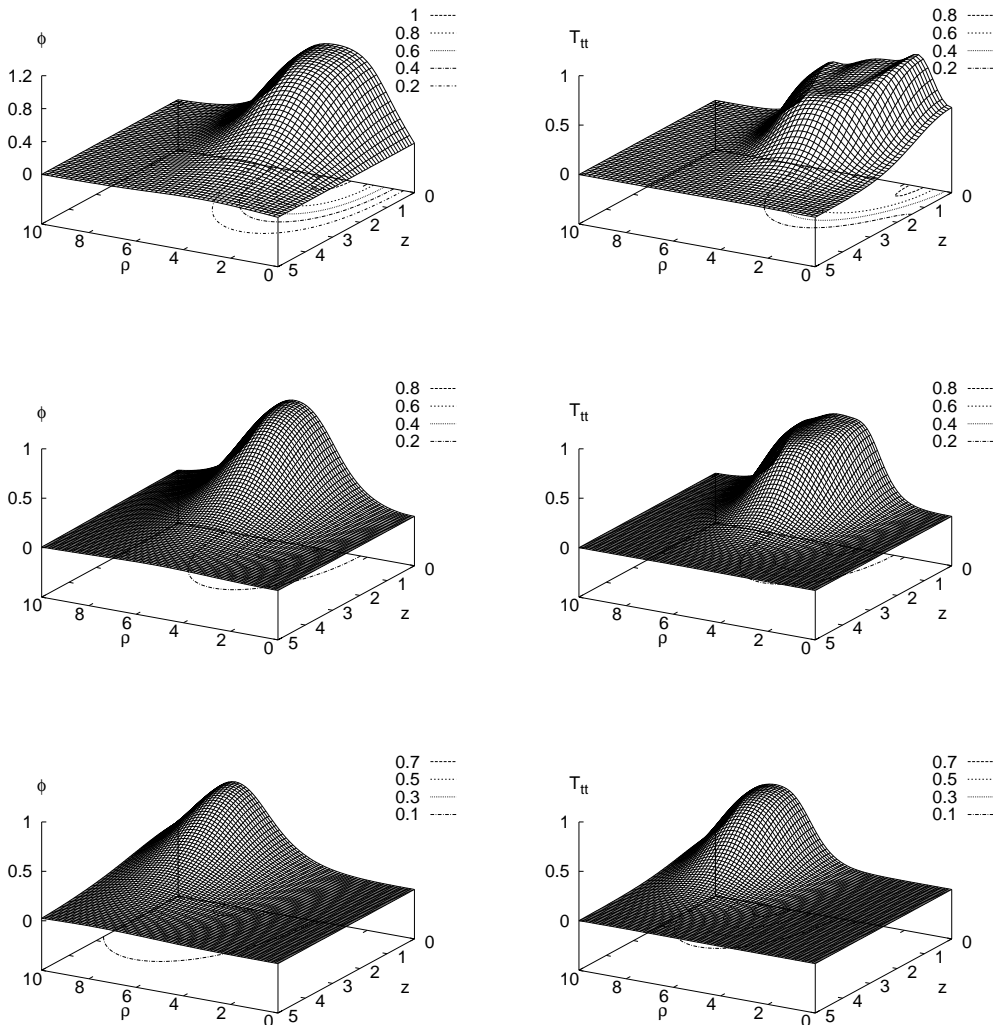


FIG. 3: The scalar field ϕ (left column) and energy density T_{tt} (right column) for rotating positive parity Q -balls with charge $Q = 410$ and $n^P = 1^+$ (upper row), 2^+ (middle row) and 3^+ (lower row) versus the coordinates $\rho = r \sin \theta$ and $z = r \cos \theta$ for $z \geq 0$.

2. Negative parity Q -balls

Turning to rotating Q -balls with negative parity, we first illustrate in Fig. 5 the scalar field ϕ and the energy density T_{tt} of Q -balls with fixed charge $Q = 720$ and $n^P = 1^-$ and 2^- . For these Q -balls the scalar field ϕ vanishes not only on the z -axis but everywhere in the xy -plane, as well. The energy density T_{tt} now typically exhibits a double torus-like structure, where the two tori are located symmetrically w.r.t. the equatorial plane [4]. When n and thus the angular momentum increases, the maxima of the energy density again shift towards larger values of the coordinate $\rho = r \sin \theta$. For the double tori of the energy density this shift with increasing n manifests as an increase of the radii of the tori in the equatorial plane.

In Fig. 6 we exhibit the charge Q versus the frequency ω_s for negative parity Q -balls with $n^P = 1^-$ and 2^- , and compare to the positive parity Q -balls. While we conclude, that for the negative parity Q -balls the limiting values ω_{\min} and ω_{\max} are retained, numerical difficulties have unfortunately prevented a more complete study.

Comparing the sets of negative and positive parity Q -balls, we conclude, that they exhibit

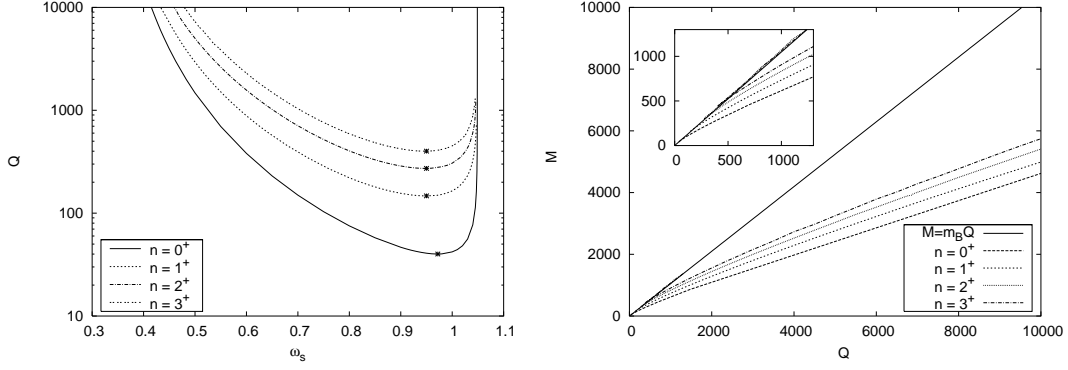


FIG. 4: Left: The charge Q versus the frequency ω_s for Q -balls with $n^P = 0^+, 1^+, 2^+, 3^+$. The asterisks mark the critical values of the charge. Right: The mass M versus the charge Q for Q -balls with $n^P = 0^+, 1^+, 2^+, 3^+$. The upper branches of the mass M are hardly discernible (on this scale) from the mass of Q free bosons, $M = m_B Q$.

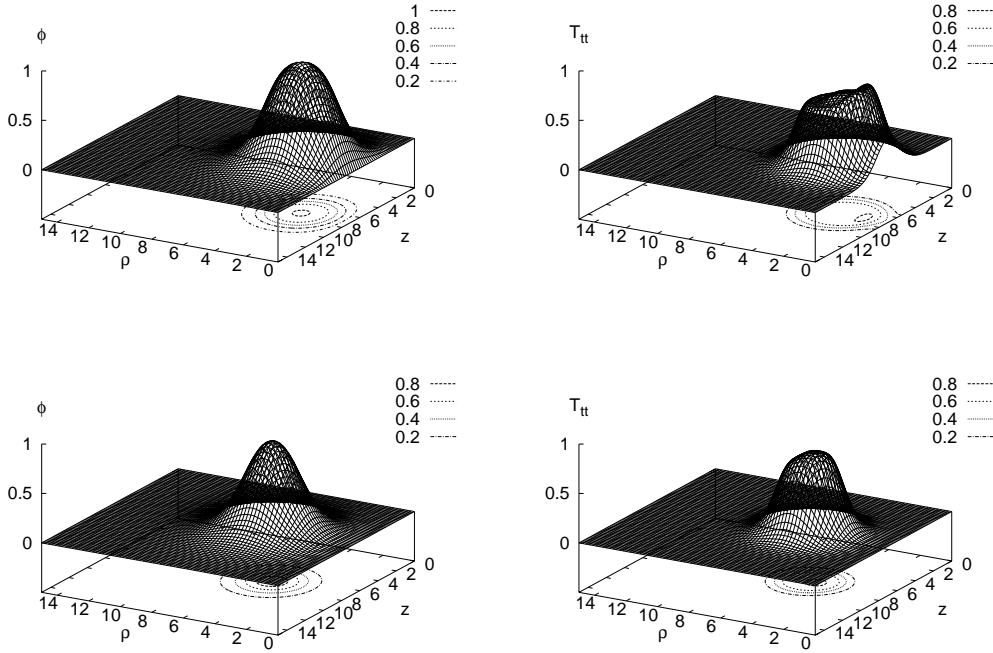


FIG. 5: The scalar field ϕ (left column) and energy density T_{tt} (right column) for rotating negative parity Q -balls with charge $Q = 720$ and $n^P = 1^-$ (upper row) and 2^- (lower row) versus the coordinates $\rho = r \sin \theta$ and $z = r \cos \theta$ for $z \geq 0$.

the same general pattern. However, concerning the magnitudes of their charges and masses, the positive parity Q -balls and the negative parity Q -balls do not quite alternate. Instead, they are ordered according to $n^P = 0^+, 1^+, 2^+, 1^-, 3^+, 2^-$, as seen in Fig. 6. Thus for Q -balls of a given charge Q , the double torus-like structure of the negative parity solutions leads to a considerably higher mass than the single torus-like structure of the positive parity solutions.

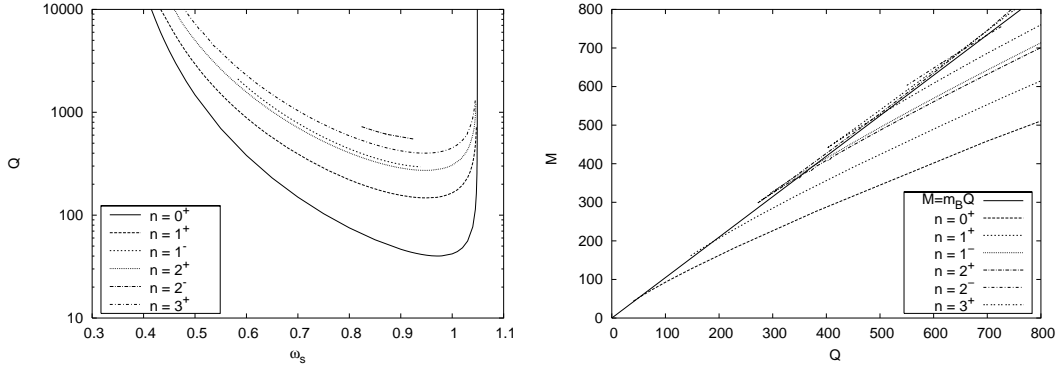


FIG. 6: Left: The charge Q versus the frequency ω_s for negative parity Q -balls with $n^P = 1^-$ and 2^- . For comparison the positive parity Q -balls with $n^P = 0^+, 1^+, 2^+, 3^+$ are also shown. Right: The mass M versus the charge Q for the same set of solutions together with the mass of Q free bosons, $M = m_B Q$.

V. BOSON STARS

A. Spherically symmetric boson stars

When the scalar field is coupled to gravity, boson stars arise (see e.g. [8, 10] for reviews). We first demonstrate the effects of gravity for spherically symmetric boson stars in Fig. 7, where we exhibit the charge Q versus the frequency ω_s for several values of the gravitational coupling constant κ .

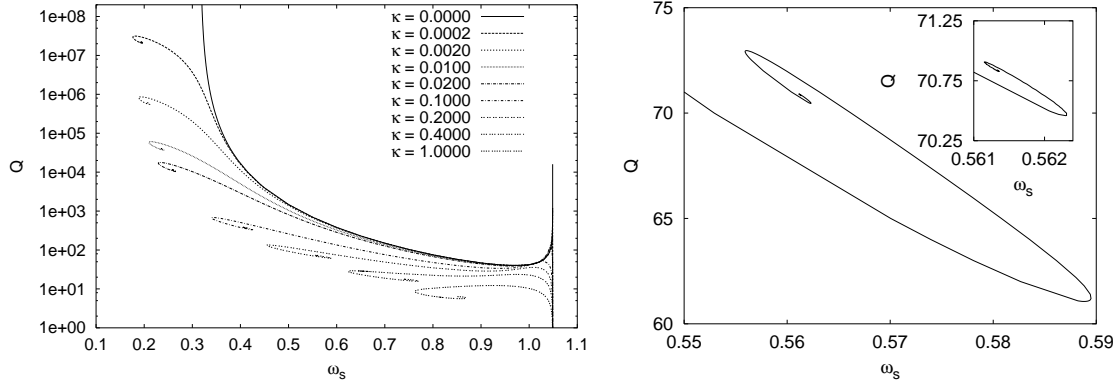


FIG. 7: Left: The charge Q versus the frequency ω_s for fundamental spherically symmetric boson stars ($k = 0$) in the full range of existence for a sequence of values of the gravitational coupling constant κ . Right: The charge Q versus the frequency ω_s in the frequency range of the spiral for the gravitational coupling constant $\kappa = 0.2$.

For solutions in curved space the frequency ω_s is also bounded from above by ω_{\max} , Eq. (39), ensuring an asymptotically exponential fall-off of the scalar field. But, unlike for flat space solutions, the charge Q does not diverge for boson stars, when ω_s approaches ω_{\max} . Instead the charge tends to zero in the limit $\omega_s \rightarrow \omega_{\max}$.

Also, for the smaller values of ω_s the solutions approach the limiting lower value ω_{\min} , Eq. (40), no longer monotonically. Instead a spiral-like behaviour arises in the presence of gravity, where the boson star solutions exhibit an inspiralling towards a limiting solution [7]. The location and size of the spiral depend on the gravitational coupling strength κ , and can be well below ω_{\min} for small values of κ (see Fig. 7) [5].

The limit $\kappa \rightarrow \infty$ is obtained by introducing the scaled scalar field $\hat{\phi}(r) = \sqrt{\kappa}\phi(r)$ [5]. Substituting $\phi(r)$ in the field equation and taking the limit $\kappa \rightarrow \infty$, the terms non-linear in $\hat{\phi}(r)$ vanish. Similarly, in the Einstein equations the terms of higher than second order

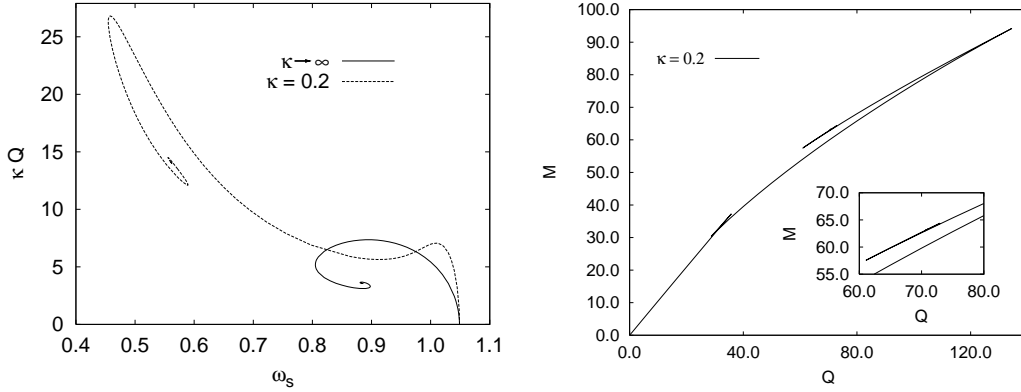


FIG. 8: Left: The scaled charge κQ versus the frequency ω_s for fundamental spherically symmetric boson stars in the limit $\kappa \rightarrow \infty$. For comparison the scaled charge κQ is also shown for $\kappa = 0.2$. Right: The mass M versus the charge Q for fundamental spherically symmetric boson stars for the value of the gravitational coupling constant $\kappa = 0.2$

in $\hat{\phi}(r)$ vanish and the dependence on κ cancels. The resulting set of differential equations is then identical to the original one, except that $\kappa = 1$ and $U(\hat{\phi}) = \lambda b \hat{\phi}^2$, reducing the potential to a mass term. This also yields a spiral pattern for the (scaled) charge $\hat{Q} = \kappa Q$, as seen in Fig. 8.

The mass M has an analogous dependence on the frequency ω_s as the charge Q . When the mass M is considered as a function of the charge Q , however, one now observes a new intricate cusp structure [5, 7]. As gravity is weakly coupled, the single cusp present in flat space (associated with the minimal value Q_{\min} of the charge) is retained. But it is supplemented by a second cusp, since in the presence of gravity the charge and the mass do not diverge for $\omega_s \rightarrow \omega_{\max}$, but tend to zero in this limit. For larger values of the gravitational coupling κ these two cusps merge and disappear. However, an additional set of cusps arises in the presence of gravity, which is due to the appearance of the spirals, and therefore only present in curved space [5, 7]. The cusp structure is illustrated in Fig. 8.

The classical stability of boson stars can be analyzed according to catastrophe theory, implying a change of classical stability at each cusp encountered [21]. In the following we refer to the main branch of solutions as the branch between the maximum of the charge and the mass (at a relatively small value of the frequency ω_s) and the local minimum of the charge and the mass (at a relatively large value of the frequency ω_s). Note, that for the flat space solutions the minimum is a global minimum, the charge and the mass assume their critical values here, while for large gravitational coupling κ the local minimum has disappeared, and the relevant minimum corresponds to the global minimum at ω_{\max} .

Along this main branch the boson star solutions are classically stable. We note though, that a small part of this main branch may become quantum mechanically unstable, when $M > m_B Q$ close to the first cusp. Since at each cusp terminating the main branch a negative mode is acquired, the solutions on the adjacent branches become classically unstable. In the spiral, the boson stars are expected to acquire at each further cusp an additional negative mode, making the solutions increasingly unstable. The physically most relevant set of solutions should thus correspond to the stable boson star solutions on the main branch.

B. Rotating Boson Stars

We now turn to rotating boson stars, which emerge from rotating Q -balls, when the gravitational coupling constant is increased from zero. We first recall the previous results on rotating positive parity boson stars with $n^P = 1^+$ [5, 6, 12] and present new results for $n^P = 2^+$. We then turn to rotating negative parity boson stars. For both cases we demonstrate and analyze the occurrence of ergoregions. We here restrict our analysis to

fundamental rotating boson stars.

1. Positive parity boson stars

We begin the discussion by recalling the main results on boson stars with $n^P = 1^+$, obtained previously [5]. For that purpose we exhibit in Fig. 9 the charge Q of 1^+ boson stars versus the frequency ω_s for several values of the gravitational coupling constant κ , including the flat space limit.

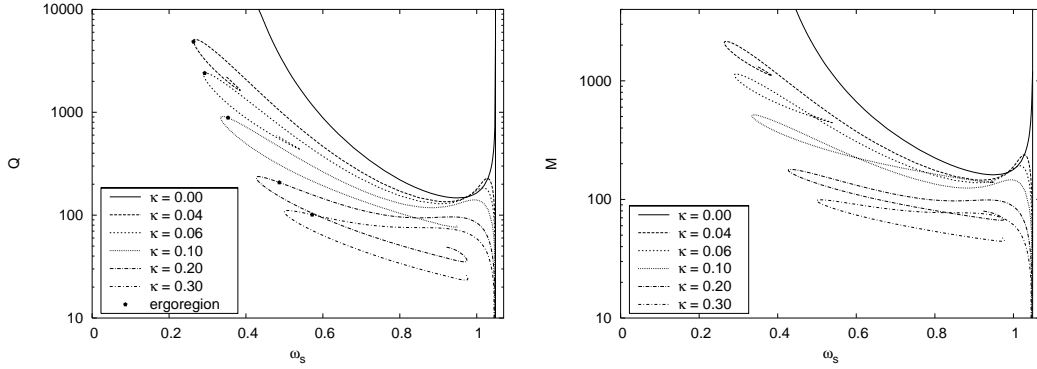


FIG. 9: Left: The charge Q versus the frequency ω_s for rotating 1^+ boson stars for several values of the gravitational coupling constant κ . Also shown are the limiting flat space values. The dots indicate the onset of ergoregions. Right: The mass M versus the frequency ω_s for the same set of solutions.

Again, the frequency ω_s of the solutions is bounded from above by ω_{\max} , Eq. (39), ensuring an asymptotically exponential fall-off of the scalar field. Also, the charge of the rotating boson stars tends to zero, when ω_{\max} is approached. Likewise, 1^+ boson stars exist only in a finite interval of the frequency ω_s , where the lower bound increases with increasing κ .

Furthermore, we observe the presence of spirals also for these rotating boson stars, i.e., the 1^+ boson stars exhibit an inspiralling towards a limiting solution just like the non-rotating boson stars. For small values of the coupling constant κ the spirals are located in the region of small frequency ω_s , for larger coupling κ the spirals shift towards larger frequencies. A good and rather complete determination of the spirals is, however, numerically often extremely difficult [5].

The mass M of the 1^+ boson stars has an analogous dependence on the frequency ω_s as the charge Q , as seen in Fig. 11. When the mass M of these rotating boson stars is considered as a function of the charge Q , we observe an analogous cusp structure as for the non-rotating boson stars [5]. In particular, for a given gravitational coupling κ , a main branch of rotating boson star solutions is present, and located between the maximum of the charge and the mass (at a relatively small value of the frequency ω_s) and the (for small gravitational coupling only local) minimum of the charge and the mass (which is not part of the spiral). Following arguments from catastrophe theory, the boson star solutions are again expected to be classically stable along this main branch.

Let us now turn to positive parity boson stars with higher quantum number n and thus greater angular momentum. We exhibit in Fig. 10 the charge Q and the mass M of 2^+ boson stars versus the frequency ω_s for several values of the gravitational coupling constant κ , including the flat space limit. Because these calculations are numerically very involved and time-consuming, we have concentrated on the main branches of these 2^+ boson stars, omitting the numerically even more involved spirals. Clearly, the 2^+ solutions show a completely analogous κ - and frequency dependence (in the regions studied) as the 1^+ solutions.

To further demonstrate the dependence of the positive parity boson stars on the rotational quantum number n , we exhibit in Fig. 11 the charge Q and the mass M as functions of the frequency ω_s for boson stars with quantum numbers $n^P = 0^+, 1^+, 2^+$ and gravitational coupling $\kappa = 0.2$.

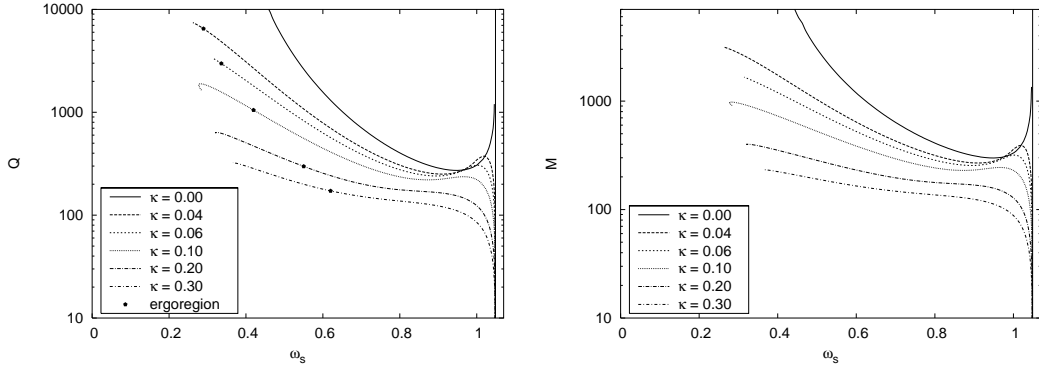


FIG. 10: Left: The charge Q versus the frequency ω_s for rotating 2^+ boson stars for several values of the gravitational coupling constant κ . Also shown are the limiting flat space values. The dots indicate the onset of ergoregions. Right: The mass M versus the frequency ω_s for the same set of solutions.

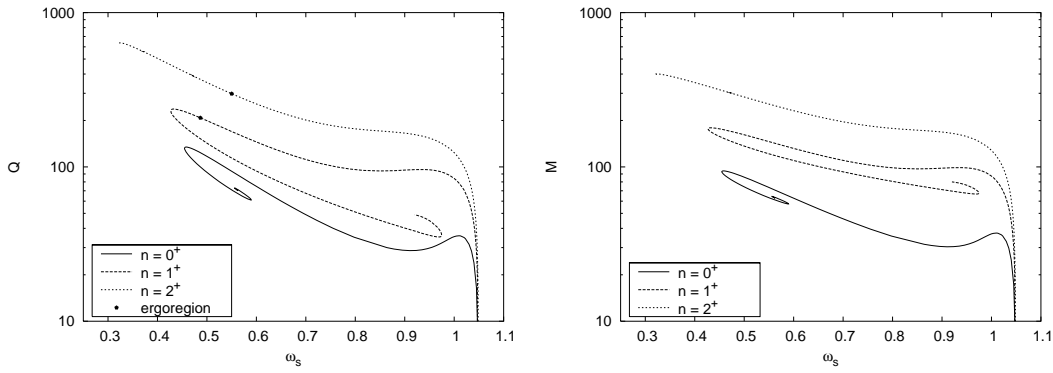


FIG. 11: The charge Q (left column) and the mass M (right column) versus the frequency ω_s for boson stars with $n^P = 0^+, 1^+, 2^+$ for the gravitational coupling $\kappa = 0.2$.

Considering the spatial structure of the solutions, the scalar field ϕ typically gives rise to a torus-like energy density T_{tt} for the rotating 1^+ and 2^+ boson stars, just as for the rotating n^+ Q -balls. Again, the torus-like shape becomes apparent by considering surfaces of constant energy density of e.g. half the respective maximal value of the energy density. As in the flat space solutions, the maximum of the energy density of the boson stars increases and shifts towards larger values of the coordinate $\rho = r \sin \theta$, when n and thus the angular momentum increases. Thus in terms of the energy density tori this again manifests as an increase of their radii in the equatorial plane with increasing n .

Rotating objects may possess ergoregions. But unlike the ergoregions of black holes, the ergoregions of regular objects like boson stars would signal the presence of an instability [13, 22–24]. This instability can be traced back to superradiant scattering, and its possible presence was put forward by Cardoso et al. [13] as an argument against various black hole doubles as potential horizonless candidates for compact dark astrophysical objects.

Therefore we now analyze the occurrence of ergoregions for rotating positive parity boson stars. The ergosurface is defined by the condition

$$g_{tt} = 0 = -f + \frac{l}{f} \sin^2 \theta \omega^2 \quad (46)$$

in the metric parametrization Eq. (16). The ergoregion resides inside this ergosurface. The presence of an ergosurface thus implies instability of the respective boson stars [13].

Examining the condition $g_{tt} = 0$ for the sets of boson star solutions, we indeed observe that rotating boson stars possess ergoregions in a large part of their domain of existence. To discuss these ergoregions, let us recall Figs. 9 and 10, where the charge Q is exhibited versus the frequency ω_s for several sets of boson stars solutions with $n^P = 1^+$ and 2^+ ,

respectively. The dots in these figures indicate the onset of ergoregions and thus ergoregion related instability at a corresponding critical frequency ω_s . The solutions to the right of the dots do not possess an ergoregion, whereas the solutions to the left of the dots as well as in the spirals do possess an ergoregion.

The onset of ergoregions thus almost always occurs on the main branch of boson star solutions, supposed to be classically stable. The presence of ergoregions then tends to diminish the physically relevant - since stable - set of solutions. As seen from the figures, the diminishment is greater for larger gravitational coupling and larger rotational quantum number n , and thus greater angular momentum. However, there always remains a part of the main branch of classically stable boson star solutions, not suffering from an ergoregion instability.

Let us now discuss the emergence and structure of ergoregions in more detail for these boson stars. For that purpose we exhibit the ergoregions of 1^+ boson stars at $\kappa = 0.1$ and 2^+ boson stars at $\kappa = 0.1$ and 0.2 in Fig. 12.

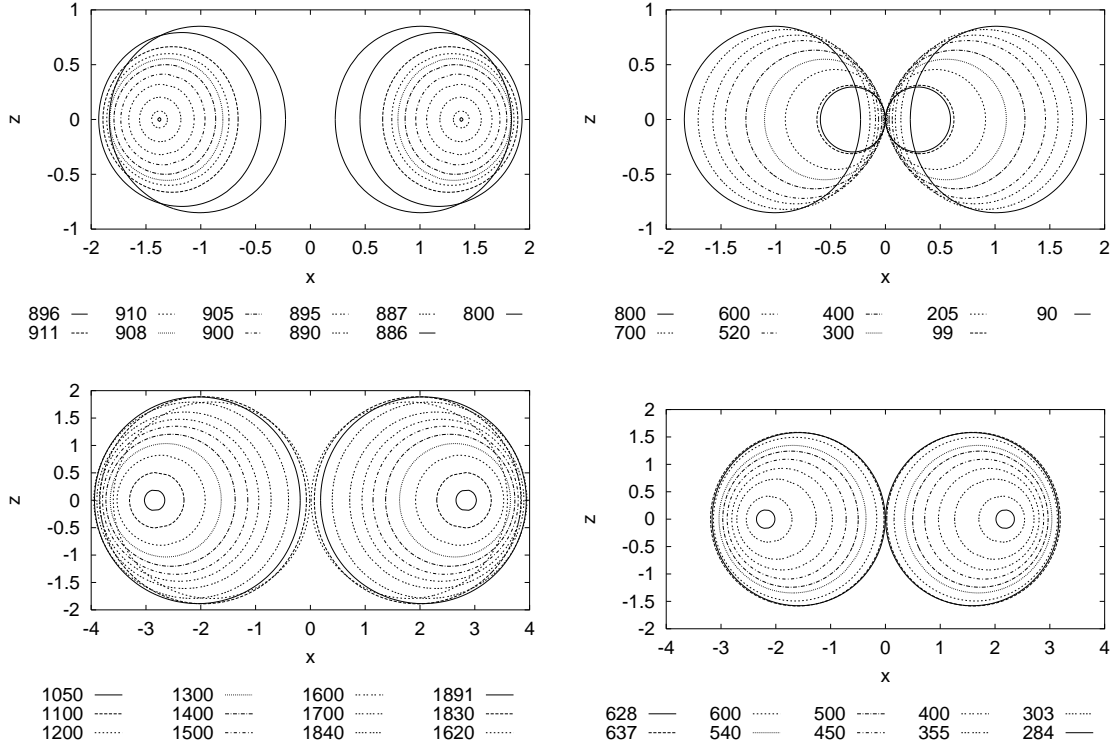


FIG. 12: Location and shape of the axially symmetric ergoregions of boson stars exhibited via cross-sections with the xz -plane: 1^+ boson stars at $\kappa = 0.1$ (upper row) and 2^+ boson stars (lower row) at $\kappa = 0.1$ (left) and at $\kappa = 0.2$ (right). The numbers in the legend indicate the respective values of the charge Q .

Beginning with the 1^+ boson stars, we observe, that at the critical frequency (where $Q \approx 986$ for $\kappa = 0.1$) the condition (46) is satisfied precisely on a circle in the equatorial plane. In the (upper left) figure, only the two points of intersection of this circle with the xz -plane are seen. As Q is increased (i.e., ω_s is decreased) the circle turns into a torus-like surface. In the figure, its intersection with the xz -plane is then seen as two small circles ($Q = 911$). From this approximately maximal value of the charge, the set of solutions now enters the first part of the spiral, where stability is lost anyway.

As the solutions evolve into the spiral the charge decreases. But the ergoregion continues to grow in size, while it remains (approximately) centered at the location, where it first arose. The ergoregion then tends towards its largest size ($Q \approx 800$), while the center of the torus of the ergoregion starts to shift inwards. Interestingly, the ergoregion is not only

topologically a torus, but also geometrically almost a torus.

As seen in the (upper right) figure, with further decreasing charge Q , the ergoregion then starts to decrease in size again, when the solutions evolve deeper into the spiral. At the same time, the center of the torus of the ergoregion continues to move further inwards. Thus the innermost part of the ergosurface gets increasingly closer to the origin, but never touches it.

The ergoregions of the set of boson stars at different values of the gravitational coupling constant κ exhibit an analogous behaviour. Likewise, the ergoregions of the sets of boson stars at higher n exhibit an analogous behaviour in the regions studied. As seen in the (lower part of the) figure, the shift of the centers of the tori of the ergoregion arises faster for $n = 2$ than for $n = 1$, yielding almost touching ergosurfaces already in the vicinity of the maximal size of the ergosurfaces.

2. Negative parity boson stars

For boson stars with negative parity we observe analogous features as for positive parity boson stars. This is illustrated in the following. We first consider 1^- boson stars for gravitational coupling $\kappa = 0.1$ and 0.2 . The dependence of their charge Q and mass M on the frequency ω_s is exhibited in Fig. 13. For $\kappa = 0.1$ a large part of the spiral could be obtained numerically.

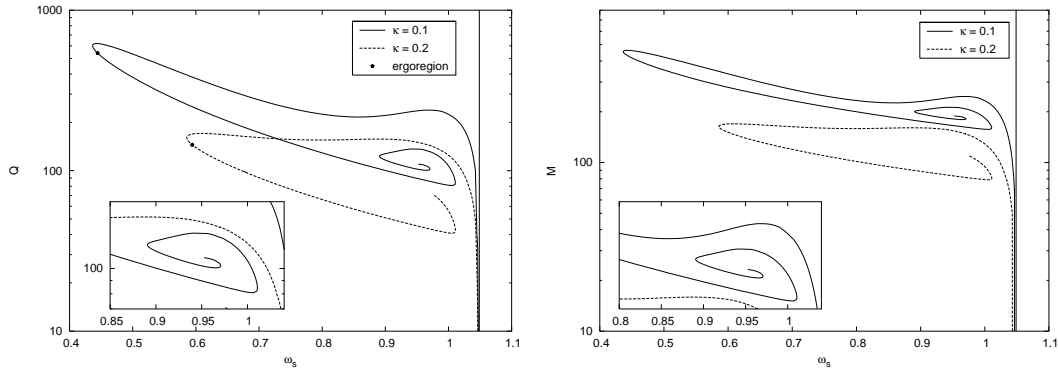


FIG. 13: The charge Q (left) and the mass M (right) versus the frequency ω_s for 1^- boson stars for gravitational coupling $\kappa = 0.1$ and 0.2 . The dots indicate the onset of ergoregions.

The mass M of negative parity boson stars exhibits the same characteristic cusp structure as the mass of positive parity boson stars, when considered as a function of the charge Q [5]. This is seen in Fig. 14 for 1^- boson stars at gravitational coupling $\kappa = 0.1$ and 0.2 .

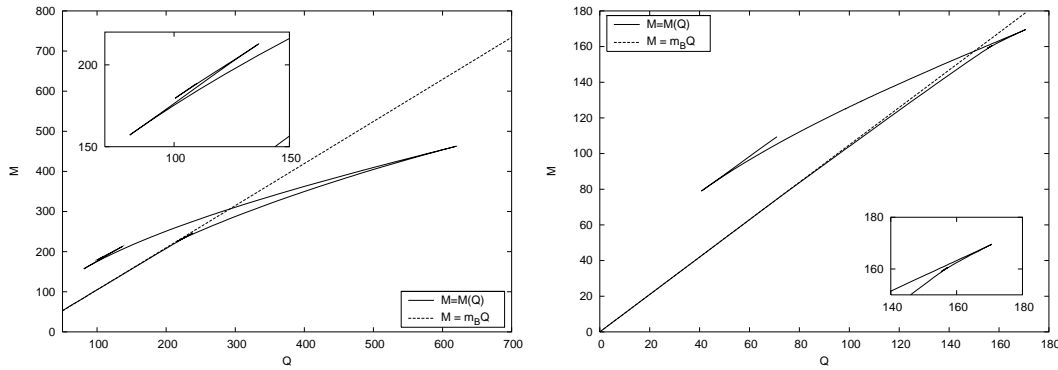


FIG. 14: The mass M versus the charge Q for 1^- boson stars for gravitational coupling $\kappa = 0.1$ (left) and 0.2 (right), together with the mass for Q free bosons, $M = m_B Q$.

In Fig. 15 we compare the 1^- boson stars to the 1^+ boson stars. In particular, we exhibit

the charge Q versus the frequency ω_s for gravitational coupling $\kappa = 0.1$ and 0.2 .

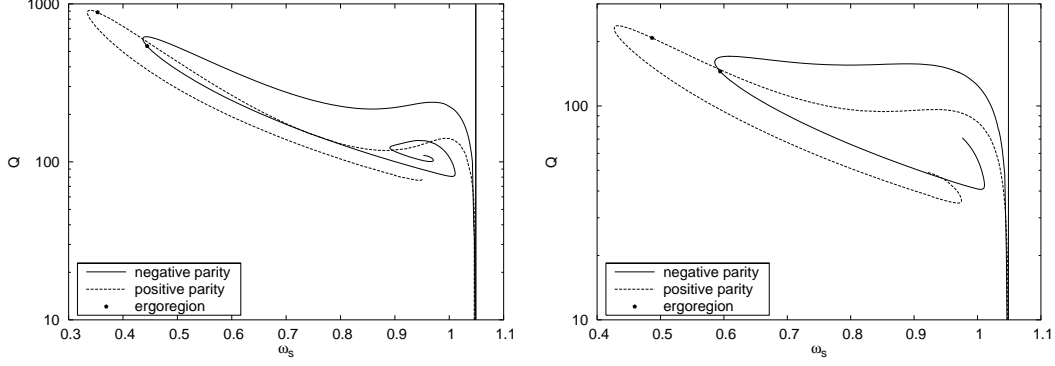


FIG. 15: The charge Q versus the frequency ω_s for 1^- boson stars and 1^+ boson stars for gravitational coupling $\kappa = 0.1$ (left) and 0.2 (right).

The n -dependence of the negative parity boson stars is demonstrated in Fig. 16. Here the charge Q is exhibited versus the frequency ω_s for coupling constant $\kappa = 0.2$. The figure also shows the mass M versus the charge Q for 2^- boson stars for $\kappa = 0.2$, exhibiting part of the cusp structure.

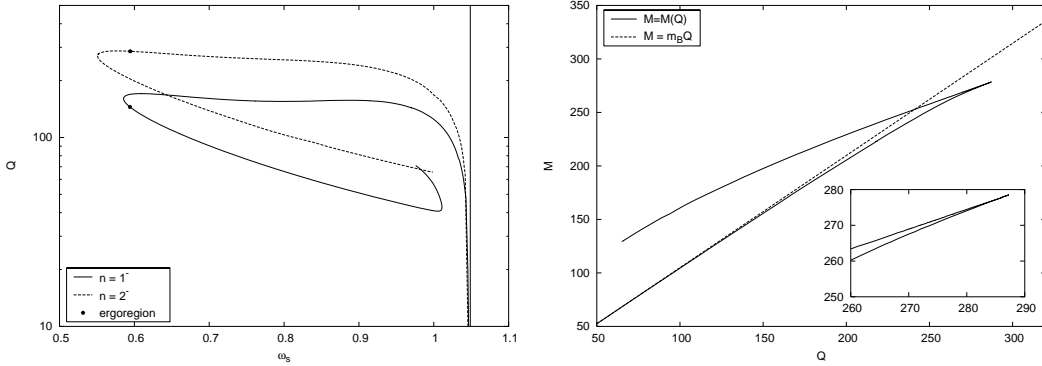


FIG. 16: Left: The charge Q versus the frequency ω_s for 1^- and 2^- boson stars for gravitational coupling $\kappa = 0.2$. The dots indicate the onset of ergoregions. Right: The mass M versus the charge Q for 2^- boson stars for gravitational coupling $\kappa = 0.2$ together with the mass for Q free bosons, $M = m_B Q$.

Considering the spatial structure of the boson stars with negative parity, the scalar field ϕ here typically gives rise to a double torus-like energy density T_{tt} for the 1^- and 2^- boson stars on the main branch, seen already in the negative parity Q -balls. As in flat space, the radii of the double tori of the energy density increase when n and thus the angular momentum increases. In the spiral the spatial structure of solutions can become more complicated, exhibiting for instance a quadruple torus-like structure.

Addressing the occurrence of ergoregions for the above sets of boson star solutions, we observe that rotating boson stars with negative parity also possess ergoregions in a large part of their domain of existence. The onset of the ergoregions for the 1^- and 2^- boson star solutions is again indicated by dots in the respective figures. Again, if the onset occurs on the main branch, then the solutions to the left of the dot and in the spiral do possess an ergoregion, while the solutions to the right of the dot do not possess an ergoregion. Likewise, if the onset occurs only in the spiral, then the solutions further down the spiral all possess ergoregions, while the other solutions do not. We demonstrate the emergence and structure of these ergoregions in more detail in Fig. 17, where we exhibit the ergoregions of 1^- boson stars at $\kappa = 0.1$ and 2^- boson stars at $\kappa = 0.2$.

Addressing first the 1^- boson stars, we observe, that at a critical value of the frequency (where $Q \approx 540$ for $\kappa = 0.1$) the condition (46) is satisfied precisely on two circles, located

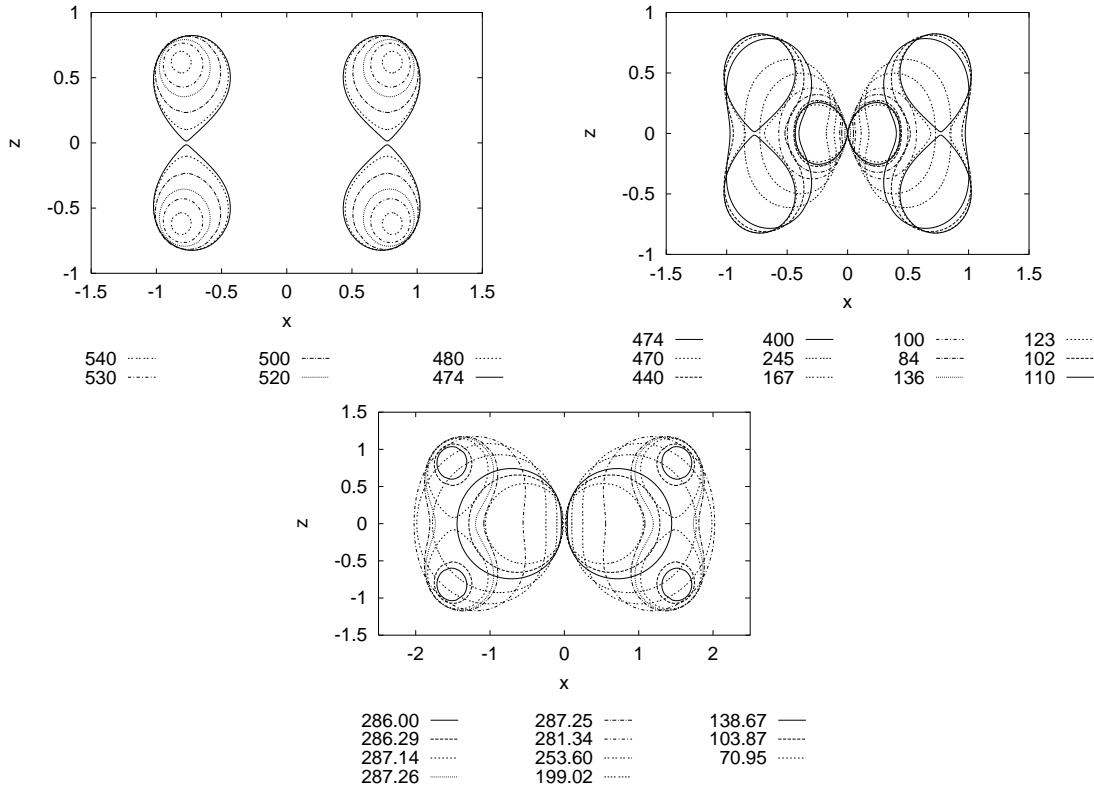


FIG. 17: Location and shape of the axially symmetric ergoregions of boson stars exhibited in the xz -plane: 1^- boson stars at $\kappa = 0.1$ (upper row) and 2^- boson stars (lower row) at $\kappa = 0.2$. The numbers in the legend indicate the respective values of the charge Q .

symmetrically w.r.t. the equatorial plane. As seen in the (upper left) figure, the circles turn into two torus-like surfaces, when Q is decreased in the first part of the spiral. The ergoregion thus consists of two disconnected tori, after it first arises.

Following the set of solutions further into the spiral, the two parts of the ergoregion increase in size until they touch at a critical value of the charge ($Q \approx 447$ for $\kappa = 0.1$) in the equatorial plane, while their centers shift only little. Beyond this critical value, the ergoregion then consists of only one connected piece, a topological torus with an 8-shaped cross-section.

As seen in the (upper right) figure, the ergoregion then rapidly changes shape and assumes a more ellipsoidal cross-section, when the solutions evolve deeper into the spiral. At the same time, the center of the torus moves further inwards. Again the innermost part of the ergosurface gets increasingly closer to the origin, but never touches it.

The ergoregions of the set of boson stars at different values of the gravitational coupling constant κ exhibit an analogous behaviour. Likewise, the ergoregions of boson stars at higher n also exhibit an analogous behaviour as seen in the (lower part of the) figure.

VI. CONCLUSIONS

We have addressed boson stars and their flat space limit, Q -balls, recalling and extending known results for positive parity solutions and presenting new negative parity solutions. Our main emphasis has been to study the general pattern displayed by these regular extended objects, to determine their domain of existence, and to investigate their physical properties.

Q -balls and boson stars exist only in a limited frequency range. Whereas both mass and charge of Q -balls assume a minimal value at a critical frequency, from where they rise monotonically towards both smaller and larger frequencies, boson stars show a different

type of behaviour. Their mass and charge tend to zero when the maximal frequency is approached, while for smaller values of the frequency the charge and mass of boson stars exhibit a spiral-like frequency dependence. The spirals end in limiting solutions with finite values of the mass and charge, which depend on the gravitational coupling constant κ .

Q -balls and boson stars possess radial excitations, which so far have only been studied for spherically symmetric solutions, and even there a systematic study has not yet been performed. Preliminary results indicate, that radially excited Q -balls and boson stars possess an analogous frequency dependence as the corresponding fundamental solutions.

Rotating Q -balls and boson stars possess an angular momentum J which is quantized in terms of the charge Q , $J = nQ$, with integer n . The positive parity solutions n^+ exhibit a torus-like energy density, while the negative parity solutions n^- exhibit a double torus-like energy density, with the two tori located symmetrically w.r.t. the equatorial plane. Clearly, the double torus-like structure of the negative parity solutions is energetically unfavourable as compared to the single torus-like structure of the positive parity solutions.

The classical stability of Q -balls and boson stars can be analyzed according to catastrophe theory, implying a change of classical stability at each cusp encountered, when the mass is considered as a function of the charge. Both type of solutions then possess classically stable branches, representing the physically most relevant sets of solutions, which in the case of boson stars have potential applications to astrophysics.

Rotating objects may possess an ergoregion. But for globally regular objects such as boson stars the presence of an ergoregion would imply an instability, associated with superradiant scattering [13, 22–24]. Thus rotating boson stars should become unstable, when they develop an ergoregion. Therefore the possible presence of ergoregions was put forward by Cardoso et al. [13] as an argument to exclude boson stars and various other black hole doubles as potential horizonless candidates for compact dark astrophysical objects.

Our analysis has shown that ergoregions can indeed be present for boson star solutions on the classically stable branch. But their presence only diminishes the set of boson star solutions with possible physical relevance (where the diminishment is greater for larger gravitational coupling and larger angular momentum), while there always remains a part of the branch of classically stable boson star solutions, not suffering from an ergoregion instability. Therefore, rotating boson stars cannot yet be excluded as potential candidates for compact astrophysical objects. It remains to be seen, whether boson stars with appropriate values of the physical parameters to fit observational data will or will not suffer from such an ergoregion instability.

Acknowledgments

We gratefully acknowledge V. Cardoso for drawing our attention to the ergoregions of boson stars. B.K. gratefully acknowledges support by the German Aerospace Center and by the DFG.

-
- [1] R. Friedberg, T. D. Lee and A. Sirlin, Phys. Rev. D13, 2739 (1976)
 - [2] S. Coleman Nucl. Phys. B262, 263 (1985) (E: B269, 744 (1986))
 - [3] T. D. Lee, and Y. Pang, Phys. Rept. 221, 251 (1992)
 - [4] M. S. Volkov and E. Wöhrner, Phys. Rev. D66, 085003 (2002)
 - [5] B. Kleihaus, J. Kunz, and M. List, Phys. Rev. D72, 064002 (2005)
 - [6] F. E. Schunck and E. W. Mielke, in *Relativity and Scientific Computing*, edited by F. W. Hehl, R. A. Puntigam and H. Ruder (Springer, Berlin, 1996), 138
 - [7] R. Friedberg, T. D. Lee and Y. Pang, Phys. Rev. D35, 3658 (1987)
 - [8] P. Jetzer, Phys. Rept. 220, 163 (1992)
 - [9] E. Mielke and F. E. Schunck, Proc. 8th Marcel Grossmann Meeting, Jerusalem, Israel, 22-27 Jun 1997, World Scientific, 1607 (1999)
 - [10] F. E. Schunck and E. W. Mielke, Nucl. Phys. B564, 185 (2000)
 - [11] E. W. Mielke, and F. E. Schunck, Proc. 8th Marcel Grossmann Meeting, Jerusalem, Israel, 22-27 Jun 1997, World Scientific, 1633 (1999)

- [12] S. Yoshida and Y. Eriguchi, Phys. Rev. D56, 762 (1997)
- [13] V. Cardoso, P. Pani, M. Cadoni and M. Cavaglia, arXiv:0709.0532 [gr-qc].
- [14] R. M. Wald, General Relativity (University of Chicago Press, Chicago, 1984)
- [15] B. Kleihaus and J. Kunz, Phys. Rev. Lett. 86, 3704 (2001)
- [16] D. Kramer, H. Stephani, E. Herlt, and M. MacCallum, Exact Solutions of Einstein's Field Equations, (Cambridge University Press, Cambridge, 1980)
- [17] B. Kleihaus and J. Kunz, Phys. Rev. Lett. 78 (1997) 2527; Phys. Rev. D57, 834 (1998)
- [18] B. Kleihaus, J. Kunz, and F. Navarro-Lérida, Phys. Rev. D66, 104001 (2002)
- [19] W. Schönauer and R. Weiß, J. Comput. Appl. Math. 27, 279 (1989)
M. Schauder, R. Weiß and W. Schönauer, The CADSOL Program Package, Universität Karlsruhe, Interner Bericht Nr. 46/92 (1992).
- [20] Y. Brihaye and B. Hartmann, arXiv:0711.1969 [hep-th].
- [21] F. V. Kusmartsev, E. W. Mielke, F. E. Schunck, Phys. Rev. D43, 3895 (1991)
- [22] J. L. Friedman, Commun. Math. Phys. 63, 243 (1978)
- [23] N. Comins and B. F. Schutz, Proc. R. Soc. Lond. A364, 211 (1978)
- [24] S. Yoshida and Y. Eriguchi, MNRAS 282, 580 (1996)